EG UK Theory and Practice of Computer Graphics (2008)
Ik Soo Lim, Wen Tang (Editors)

A Lemon is not a Monstar: visualization of singularities of symmetric second rank tensor fields in the plane

J. Liu[1], W.T. Hewitt[2], W.R.B. Lionheart[3], J. Montaldi[3] and M. Turner[2]

Jia.Liu@hull.ac.uk and {w.t.hewitt, bill.lionheart, j.montaldi, martin.turner}@manchester.ac.uk
[1] Department of Computer Science, University of Hull
[2] Research Computing Services, University of Manchester
[3] School of Mathematics, University of Manchester

Abstract

In the visualization of the topology of second rank symmetric tensor fields in the plane one can extract some key points (degenerate points), and curves (separatrices) that characterize the qualitative behaviour of the whole tensor field. This can provide a global structure of the whole tensor field, and effectively reduce the complexity of the original data. To construct this global structure it is important to classify those degenerate points accurately. However, in existing visualization techniques, a degenerate point is only classified into two types: trisector and wedge types. In this work, we will apply the theory from the analysis of binary differential equations and demonstrate that, topologically, a simple degenerate point should be classified into three types: star (trisector), lemon and monstar. The later two types were mistakenly regarded as a single type in the existing visualization techniques.

1. The introduction

Symmetric second rank tensor data is central to many applications in both physics and engineering. In recent years an increasing quantity of tensor data has been produced in scientific experiments and engineering simulations. For example, the velocity gradient and rate-of-strain tensor in fluid flow, the stress and strain tensors in solid mechanics, or the diffusion tensor in medical physics. Scientists and engineers face the problem of understanding these significant quantities of important data. The development of new algorithms for the visualization of tensor data is particularly challenging, not least because of the complexity of the data itself.

The visualization techniques for tensor fields can be classified into two main categories: one is to map the tensor data onto the geometric parameters of the icons such as hyperstreamlines [DH92], and the other is the automatic extraction of the features—namely, singularities, the topological features—of the tensor data [Del94] [LLH97]. The icon based visualization can provide good visual cue of the data directly, but with the increase of the volume of data, visual clutter can become a very serious problem. Furthermore, it can be difficult to extract useful information from a large number of icons resulting from the large volume of data. By using feature based approach to extract the interesting information from the data directly, it will largely reduce the information to be processed and the visual clutter.

The visualization of the topology of tensor fields was first introduced by Delmarcelle [DH94] to the visualization community in 1994 and analysis of the topology of tensor fields is an extension of the analysis of the topology of vector fields [HH89] [HH90] [HH91]. Similar to analysis of topology in vector fields, key points (degenerate points) are extracted and curves (separatrices) are produced that characterize the whole tensor field into different qualitative behaviour. This provides a way to extract global structure information from tensor data whilst reducing the complexity of the original data. These degenerate points and separatrices consist of a so-called *topological structure* of the tensor field.

In order to construct the topological structure of the tensor field in the plane accurately, it is important to classify degenerate points. However, in the existing visualization techniques, a degenerate point is only classified into two types: trisector and wedge types. In this paper, we will apply theory from the analysis of binary differential equations and

demonstrate that a simple degenerate point topologically should be classified into three types: star (trisector), lemon and monstar. A lemon is not a monstar, but the two were classified as a single type, known as the wedge type in the existing visualization literature.

2. Analysis of the topology of tensor fields

Whilst the analysis of the topology of vector fields is centered on the analysis of critical points, the analysis of the topology of tensor fields is based on the analysis of degenerate points, which are points where the two eigenvalues are equal. At each non-degenerate point of the domain the tensor field has two distinct eigenvalues, and while it is tempting to choose a unit eigenvector for each of these, this is not usually possible in a globally consistent manner. One therefore considers *line fields* that are the one dimensional eigenspaces of the tensor at each point; since the tensor field is symmetric these are always orthogonal, except at degenerate points where they are not defined. The integral curves of these line fields are called the characteristic curves or integral curves of the tensor field. Note that it is possible to distinguish the two characteristic curves globally (where they are defined), for example one has a larger eigenvalue than the other.

An index for a tensor field can be defined in a similar way to the index of a vector field [ALGM73].

Definition 1 (tensor index) The tensor index $I_T(\gamma)$ of a Jordan curve [Car78] γ relative to a tensor field $T:\mathbb{R}^2\to\mathbb{R}^2\otimes\mathbb{R}^2$ is defined as;

$$I_T(\gamma)=\frac{\Delta\theta}{2\pi}$$

where $\Delta\theta$ is the total change in the angle θ between one of the characteristic lines and the x axis, as the curve γ is traversed once in an anticlockwise direction.

Since the two characteristic lines are always orthogonal, they rotate by the same amount so that this index is the same for each of the line fields. Unlike the index for a vector field, here the index is only a half-integer. This is because $\Delta\theta$ is only a multiple of π not of 2π.

Given a symmetric tensor field on $\mathbb{R}^2$ with respect to a basis,

$$\begin{pmatrix} T_{11}(x,y) & T_{12}(x,y)\\ T_{12}(x,y) & T_{22}(x,y)\end{pmatrix}, \tag{1}$$

one can obtain the following equation for the tensor index calculation

$$I_T(\gamma)=\frac{1}{2\pi}\oint_\gamma \frac{(T_{11}-T_{22})\mathrm{d}T_{12}-T_{12}\mathrm{d}(T_{11}-T_{22})}{(T_{11}-T_{22})^2+4T_{12}^2} \tag{2}$$

Definition 2 (tensor index of a degenerate point) Let Ω be an open subset of $\mathbb{R}^2$, and $\mathbf{x}_0\in\Omega$ is an isolated degenerate point of the tensor field $T:\mathbb{R}^2\to\mathbb{R}^2\otimes\mathbb{R}^2$. The index $I_T(\mathbf{x}_0)$ of a degenerate point $\mathbf{x}_0$ of line fields of a symmetric tensor field is defined as the index of any Jordan curve γ containing $\mathbf{x}_0$ in its interior such that there are no other degenerate points of the field either inside or on γ

$$I_T(\mathbf{x}_0)=I_T(\gamma)$$

In this paper, from now on we will usually use the more familiar "eigenvector" rather than "characteristic lines".

However, before Delmarcelle's theory, Bruce *et al.* [BF89] proposed the local classification of solution curves of line fields, determined by eq. (3):

$$a(x,y)(\mathrm{d}y)^2+2b(x,y)\mathrm{d}y\mathrm{d}x-a(x,y)(\mathrm{d}x)^2=0 \tag{3}$$

where $a(x,y)$ and $b(x,y)$ are smooth functions which both vanish at $\mathbf{0}\in\mathbb{R}^2$.

Given a tensor field as defined in eq. (1), one can show that the line fields $\begin{pmatrix}\mathrm{d}x\\ \mathrm{d}y\end{pmatrix}$ of this tensor field satisfy the binary differential equation:

$$T_{12}((\mathrm{d}y)^2-(\mathrm{d}x)^2)+(T_{11}-T_{22})\mathrm{d}y\mathrm{d}x=0 \tag{4}$$

Comparing eq. (4) to (3), one can obtain

$$a(x,y)=T_{12}(x,y), b(x,y)=(T_{11}(x,y)-T_{22}(x,y))/2 \tag{5}$$

One can also show that the two real eigenvalues of a symmetric 2×2 matrix represented by eq. (1) are equal at (x_0,y_0), i.e. (x_0,y_0) is a degenerate point, if

$$\begin{cases}(T_{11}(x_0,y_0)-T_{22}(x_0,y_0))/2=0\\ T_{12}(x_0,y_0)=0\end{cases} \tag{6}$$

Therefore the problem of the local classification of the degenerate point of tensor fields in Delmarcelle's method is actually the same as the problem of the local classification of solution curves of eq. (3), where a and b both vanish at degenerate points.

Both Delmarcelle and Bruce have proved that the local classification of line fields or degenerate points can be determined by the constants:

$$\begin{aligned} a_1&=\partial a/\partial x(x_0,y_0), a_2=\partial a/\partial y(x_0,y_0)\\ b_1&=\partial b/\partial x(x_0,y_0), b_2=\partial b/\partial y(x_0,y_0)\end{aligned} \tag{7}$$

Thus $a(x,y)$ and $b(x,y)$ at (x_0,y_0) can be approximated by:

$$\begin{aligned} a(x,y)&=a_1x+a_2y+O(2)\\ b(x,y)&=b_1x+b_2y+O(2)\end{aligned} \tag{8}$$

when $\delta=a_1b_2-a_2b_1\neq 0$. The whole field can be separated into different regions by the root lines of a cubic equation $C_3(p_1)$:

$$C_3(p_1)=a_2p_1^3+(2b_2+a_1)p_1^2+(-a_2+2b_1)p_1-a_1 \tag{9}$$

The cubic equation (9) will have one or three distinct real roots ($\delta=a_1b_2-a_2b_1\neq 0$). Delmarcelle showed that the degenerate point can be classified into two types based on the sign of δ (Delmarcelle originally defined $\delta=a_2b_1-a_1b_2$.

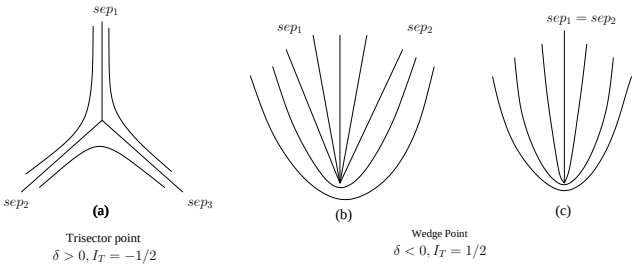

Figure 1: *Delmarcelle's classification of degenerate points reproduced from [Del94] (sep_i denotes the separatrices arising from each type of degenerate points)*

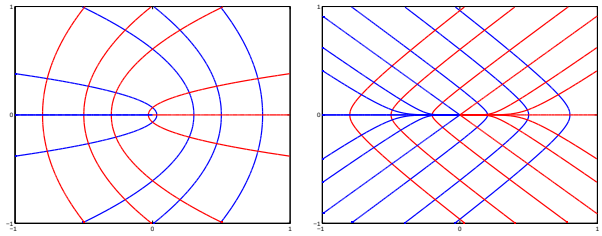

(a)Lemon $\begin{pmatrix} x & y \\ y & -x \end{pmatrix}$ (b)Monstar $\begin{pmatrix} \frac{1}{4}x & 3y \\ 3y & -\frac{1}{4}x \end{pmatrix}$

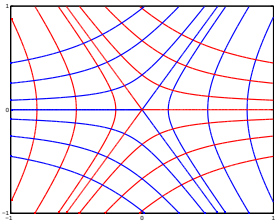

(c) Star $\begin{pmatrix} x & -y \\ -y & -x \end{pmatrix}$

Figure 2: *Three types of solution curves of binary differential equations*

We use Bruce's definition here); When $\delta > 0$, the degenerate point is called a trisector point and has an index $-\frac{1}{2}$; When $\delta < 0$, the degenerate point is called a wedge point and has an index $+\frac{1}{2}$. Therefore, the degenerate point can be classified either by calculating its tensor index or δ (see Figure 1). Bruce classified the solution curves into three types: lemon, star and monstar as shown in Figure 2 (The terminology is due to Berry and Hannay [BH77]). The blue and red solution curves are orthogonal to each other. The same set of data can be visualized using textures as shown in Figure 3. Here the white lines on top of each texture [LPTH05] represent the solution lines in each case.

Comparing Figures 2 and 1, Delmarcelle defined both lemon and monstar as a single type—a wedge point. For the wedge point, two cases exist, as shown in Figure 1 (b) and (c). In Figure 1 (b) there are two separatrices sep_1 and sep_2, and in Figure 1 (c) there is just one separatrix $sep_1 = sep_2$. However as shown in Figures 2 and 3, the topology of lemon and monstar cases is quite different, thus they can not be regarded as a single type, even though they both have an index of $+\frac{1}{2}$. Both monstar and star cases have three root lines, although the former is contained in a right angle and the other is not. In the lemon case, the cubic $C_3(p_1)$ has just one real root. Therefore, Delmarcelle's method is not sufficient

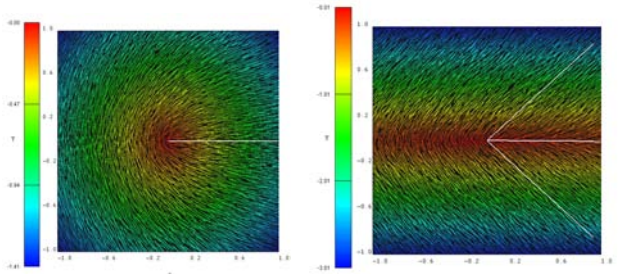

(a)Lemon (b)Monstar

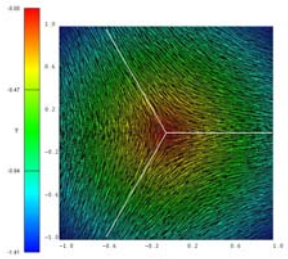

(c) Star

Figure 3: *One of the two line fields of the tensor fields defined in Figure 2 is visualized by textures. The white lines are root lines of cubic $C_3(p_1)$. (Textures are coloured by the corresponding eigenvalue)*

for differentiating lemon and monstar. Bruce *et al.* showed that the field of pairs of characteristic lines lifts to define a vector field on a new surface which projects back down to $\mathbb{R}^2$ [BF89]. The zeros of this vector field (critical points) are $(0, p_1)$, and p_1 are the roots of eq. (9). The eigenvalues (λ_1, λ_2) of the Jacobian matrices of these critical points are calculated (see Proposition 1.5 in [BF89] for the proof):

$$\lambda_1 = 2(a_2 p_1^2 + (a_1 + b_2)p_1 + b_1)$$
$$\lambda_2 = -(3a_2 p_1^2 + 2(a_1 + 2b_2)p_1 + (2b_1 - a_2)) \qquad (10)$$

where p_1 is one of roots of eq.(9). It is known that critical points of vector fields can be classified by the eigenvalues of their Jacobian matrices (see Figure 4). By classifying the critical points of the lifted vector field, one can classify the degenerate point of tensor fields:

- If the lifted vector field has just one critical point which is

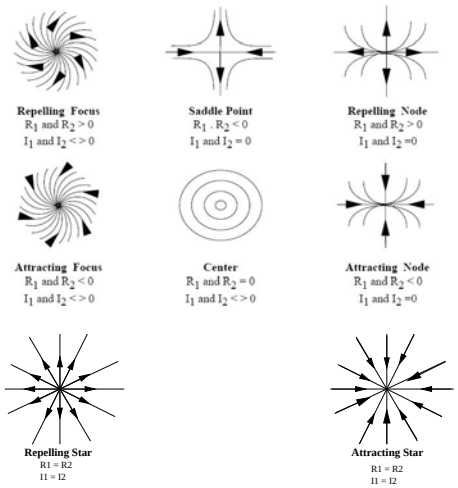

Figure 4: *The classification of critical points, where R_i and I_i represent the real and imaginary parts of the eigenvalue $\lambda_i, i = 1,2$.*

a saddle, the degenerate point of the tensor field is lemon type;

- If the lifted vector field has three critical points and all are saddles, the degenerate point of the tensor field is star type;
- If the lifted vector field has three critical points, two saddles and one node, the degenerate point of the tensor field is monstar type.

For example, in the monstar case shown in Figure 2 (b), the symmetric tensor field with respect to a basis can be represented by the matrix:

$$\begin{pmatrix} \frac{1}{4}x & 3y \\ 3y & -\frac{1}{4}x \end{pmatrix} \tag{11}$$

The eigenvector satisfies the binary differential equation:

$$3ydy^2 - (\frac{1}{4}x + \frac{1}{4}x)dydx - 3ydx^2 \tag{12}$$

One can obtain $a_1 = 0, a_2 = 3, b_1 = 1/4, b_2 = 0$ (using eqs. (3) and (7)), thus the cubic $C_3(p_1) = 3p_1^3 - \frac{5}{2}p_1$ has three roots: $0, \sqrt{5/6}, -\sqrt{5/6}$. For each critical point of the lift vector field, its two eigenvalues λ_1 and λ_2 (see eq. (10)) are $0.5, 2.5$ and $5.5, -5$ and $5.5, -5$ respectively. These three critical points are one node and two saddles (see Figure 4). Similarly one can check that for the lemon case in Figure 2 (a), the lift vector field has just one saddle.

Furthermore, if $p_1 = y/x$, then eq. (9) can be written in a cubic form, $m_1x^3 + 3m_2x^2y + 3m_3xy^2 + m_4y^3$ $(m_1, \cdots m_4, \in \mathbb{R})$. In the case of $C_3(p_1)$ having one or three real roots, the cubic form can be classified as either an elliptic (three real and distinct roots) or a hyperbolic (one real root, two complex conjugate roots) case [Por01]. Therefore, both the monstar and star can also be regarded as an hyperbolic type, whilst the lemon is an elliptic type.

In order to further analyse the relationship between lemon, star and monstar types, the cubic form can be denoted by:

$$\alpha z^3 + 3\bar{\beta}z^2\bar{z} + 3\beta z\bar{z}^2 + \bar{\alpha}\bar{z}^3 \tag{13}$$

where $z = x + iy \in \mathbb{C}$ and α and β both elements of $\mathbb{C}$. With a proper coordinate transformation ($z = \alpha^{1/3}z$), eq. (13) can be transformed into

$$z^3 + 3\bar{\beta}z^2\bar{z} + 3\beta z\bar{z}^2 + \bar{z}^3 \tag{14}$$

when $\alpha \neq 0$. Therefore, any cubic form in $\mathbb{R}^2$ can be represented by β in a complex plane. When $\alpha = 0$, eq. (13) becomes $3\bar{\beta}z^2\bar{z} + 3\beta z\bar{z}^2$, and can be considered as lying at the infinity of the complex plane. Porteous [Por71] [Por83] [Por01] has shown that a cubic from within the complex plane can be classified as shown in Figure 5. The tricuspidal curve is defined by $\beta = -\gamma^2 - 2\bar{\gamma}$, where $|\gamma| = 1$. For lemon type, the β values of the cubics will lie outside this curve. Inside this curve but outside the circle $|\beta| = 1$, the cubics will be of monstar type, inside the circle the cubics will be of star type.

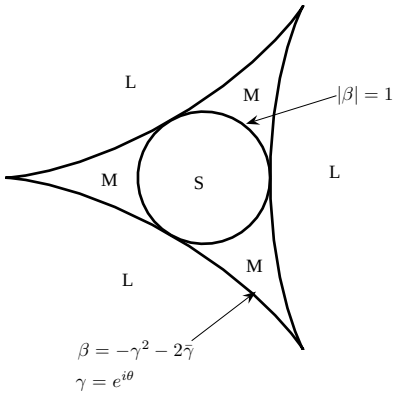

Figure 5: *The relationship of lemon (L), monstar (M) and star (S) in the complex plane*

All of the above classifications assume $\delta \neq 0$. When $\delta = 0$, there is a higher order degenerate point such that a first order Taylor expansion of $a(x,y)$ and $b(x,y)$ (see eq.(8)) is no longer sufficient; higher order terms must be included. However, this is beyond the scope of this paper. More details regarding to higher order degenerate points can be found elsewhere [Liu08].

In the next section, we will discuss how to apply those theories to the visualizations.

3. Classifying the degenerate point in the visualization

In section 2, we introduced the idea that a degenerate point could be classified into three types—lemon, monstar and star. The first two classifications both have indices of $+1/2$, whilst the latter one has an index of $-1/2$. Thus to classify the type of a linear degenerate point, its tensor index can first be calculated. If the tensor index is $+1/2$, then Bruce's result will be used to differentiate lemon and monstar, which in the work of Delmarcelle were denoted by a single classification—wedge. The detailed algorithm for classifying linear degenerate points is as follows:

step 0 To compute the partial derivatives values a_1, a_2, b_1, b_2 at a degenerate point (x_0, y_0) in eq. (7) using the Surface Spline (SSPL) [HD72] [Yu01] method directly;

step 1 To compute the tensor index, if the index is $-\frac{1}{2}$, the degenerate point is classified as star type, and stop. Otherwise, go to step 2;

step 2 To solve the cubic equation eq. (9) and to obtain one or three critical points of the lifted vector field;

step 3 To compute the eigenvalues λ_1 and λ_2 of Jacobian matrix at these critical points obtained in step 2 using eq. (10). If there is just one saddle point, then the degenerate point is classified as lemon, otherwise the degenerate point is classified as monstar.

To compute the tensor index in step 1, one possible approach involves evaluating the integral shown in eq. (2). However, in most cases the tensor data is not analytical and eq. (2) can not be applied. A direct computation from the definition of the tensor index is adopted here. For example, in Figure 6 (a), there is a degenerate point O at $(0.68, -0.59)$. A circle can be obtained around the degenerate point as long as there are no other degenerate points on or inside this circle. If P_i and P_{i+1} $(i = 1, 2, \ldots, n)$ are two anticlockwise consecutively sampled points on the circle and n is the total number of sample points on the circle, then the eigenvectors $\mathbf{v}_i$ and $\mathbf{v}_{i+1}$ can be evaluated at these sample points (The obtained eigenvector $\mathbf{v}_i$ of a 2×2 matrix points in one direction only, but by multiplying the vector by -1, one can obtain the bivalued eigenvector.). We note that these eigenvectors are bidirectional, as shown in Figure 6, so that the angle change of eigenvectors from P_i to P_{i+1} can be calculated by:

$$\Delta\phi_i = \min(\text{acos}(\mathbf{v}_i \cdot \mathbf{v}_{i+1}), \text{acos}(\mathbf{v}_i \cdot -\mathbf{v}_{i+1}))$$

Assuming that θ_i is the angle of eigenvector $\mathbf{v}_i$ makes with the x axis (positive direction), if $\theta_{i+1} > \theta_i$, then the eigenvector is rotated anticlockwise, otherwise the eigenvector is rotated clockwise. The former results in positive angle changes and the later result in negative angle changes. Furthermore, positive angle changes result in a positive index, whilst negative angle changes result in a negative index. Finally, the total change of angle is the sum of $\Delta\phi_i$:

$$\phi_{total} = \sum_{i=1}^{n} \Delta\phi_i \tag{15}$$

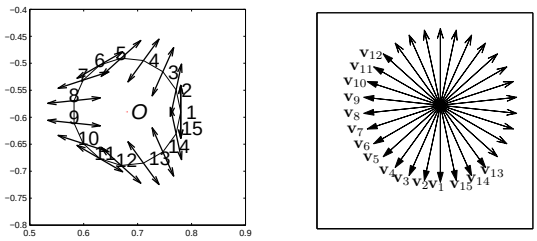

(a) (b)

Figure 6: *Computation of the tensor index around a degenerate point. Two different arrow heads are used in (b). One arrow head (on the left in the image) is for $\mathbf{v}_i$, and the other is for $-\mathbf{v}_i$. Note from $\mathbf{v}_{12}$ to $\mathbf{v}_{13}$, the angle change is calculated as $\Delta\phi_{12} = acos(\mathbf{v}_{12} \cdot -\mathbf{v}_{13})$.*

Therefore, the index of the degenerate point will be

$$I_T = \phi_{total}/2\pi$$

In the example shown in Figure 6 (a), there are 15 samples on the circle i.e., a total of 15 eigenvectors are evaluated, one at each point. Shifting the centre of these eigenvectors to the same point as shown in Figure 6 (b), we can see that along the circle the anticlockwise eigenvectors $\mathbf{v}_1$ to $\mathbf{v}_{15}$ have rotated through a total angle of $-\pi$. Therefore the index for this degenerate point will be $-\frac{1}{2}$, i.e. a star type degenerate point.

4. Results

In order to test the accuracy of the proposed algorithm, it was necessary to design synthetic tensor data with known topological features. The design of the test tensor data adopted the following heuristic: from Theorem A.1 [SHK*97] (see Appendix A), one can define a vector field with specified order and location with

$$\mathbf{v} = E(z, \bar{z})\mathbf{e}_1 \tag{16}$$

where $E : \mathbb{C}^2 \to \mathbb{C}$ is a complex valued function on $\mathbb{C}^2$. Eq. (16) can also be represented as (Refer to eqs. (27) to (29) in Appendix A)

$$\begin{pmatrix} v_1 \\ v_2 \end{pmatrix} = \begin{pmatrix} \mathrm{R}(E) \\ -\mathrm{I}(E) \end{pmatrix} \tag{17}$$

Here, $\mathrm{R}(E)$ stands for the real part of E, and $\mathrm{I}(E)$ stands for the imaginary part of E.

A symmetric rank-2 tensor on $\mathbb{R}^2$ with respect to an arbitrary basis can be represented as:

$$T = \begin{pmatrix} T_{11} & T_{12} \\ T_{12} & T_{22} \end{pmatrix}$$

which can be further decomposed into two parts:

$$T = U + D \tag{18}$$

where

$$U = \begin{pmatrix} (T_{11}+T_{22})/2 & 0 \\ 0 & (T_{11}+T_{22})/2 \end{pmatrix} \quad (19)$$

and

$$D = \begin{pmatrix} (T_{11}-T_{22})/2 & T_{12} \\ T_{12} & -(T_{11}-T_{22})/2 \end{pmatrix} \quad (20)$$

U and D are also known as *isotropic* and *deviatoric* parts of a matrix T. Since a general symmetric tensor and its deviatoric part have the same set of eigenvectors [LLH97], the computation of eigenvectors for the deviatoric part is sufficient for a general matrix. Therefore, only the deviatoric part of a general matrix is required for the design of synthetic tensor data. This is sufficient for our purpose, the testing of our algorithms for the extraction of degenerate points and the subsequent construction of topological skeletons of the tensor fields. For any real tensor data on $\mathbb{R}^2$, T_{11}, T_{12}, and T_{22} will be known in advance. If

$$\begin{cases} (T_{11}-T_{22})/2 = \mathrm{R}(E) \\ T_{12} = -\mathrm{I}(E) \end{cases}$$

where $E : \mathbb{C}^2 \to \mathbb{C}$ is a complex valued function on $\mathbb{C}^2$, as introduced in appendix A (see eq. (28)), then the tensor field T on $\mathbb{R}^2$ with respect to a basis can be defined as follows:

$$\begin{pmatrix} \mathrm{R}(E) & -\mathrm{I}(E) \\ -\mathrm{I}(E) & -\mathrm{R}(E) \end{pmatrix} \quad (21)$$

which has degenerate points when eq. (6) is satisfied, that is

$$\begin{cases} \mathrm{R}(E) = 0 \\ \mathrm{I}(E) = 0 \end{cases}$$

Therefore, all zeros within the vector field $\mathbf{v}$ (see eq. (17)) specify the degenerate points for the tensor field T defined in eq. (21).

$$E = (z-(-0.5-0.2i))(\bar{z}-\overline{(-0.7-0.7i)}) \left(\frac{1}{4}(x-0.7)-3(y-0.4)i\right) \quad (22)$$

which consists of three different types of linear degenerate points, at locations $(-0.7,-0.7)$, $(-0.5,-0.2)$ and $(0.7,0.4)$. Note that the third component of E:

$$F_3 = \left(\frac{1}{4}(x-0.7)-3(y-0.4)i\right)$$

is designed from the monstar in Figure 2 (b), since $\mathrm{R}(F_3) = \frac{1}{4}(x-0.7)$ and $-\mathrm{I}(F_3) = 3(y-0.4)i$. This leads to a tensor field:

$$\begin{pmatrix} \mathrm{R}(F_3) & -\mathrm{I}(F_3) \\ -\mathrm{I}(F_3) & -\mathrm{R}(F_3) \end{pmatrix} = \begin{pmatrix} \frac{1}{4}(x-0.7) & 3(y-0.4) \\ 3(y-0.4) & -\frac{1}{4}(x-0.7) \end{pmatrix} \quad (23)$$

Figure 7 (a) and (b) show the topological structures extracted using the existing visualization technique and our algorithm respectively. It can be seen that at the location $(0.7,0.4)$ there is a monstar in Figure 7 (a), which is classified into a wedge ('W') type in Figure 7 (b). Due to this classification, there is a missing separatrix in Figure 7 (a). Therefore the topological structure is misleading. It is important to construct the correct topological structure to help the users to understand the data in the sense that Figure 7 (b) visualizes the structure of the underlying data correctly. Using the space filling textures in Figure 7, it also demonstrates different eigenvector patterns in each subregion separated by these separatrices (white curves) without visual clutter. By overlaying the topological structure on top of it, it will enable the user to quickly focus on the interesting features in the data, at the same time as filling in the gaps between separatrices.

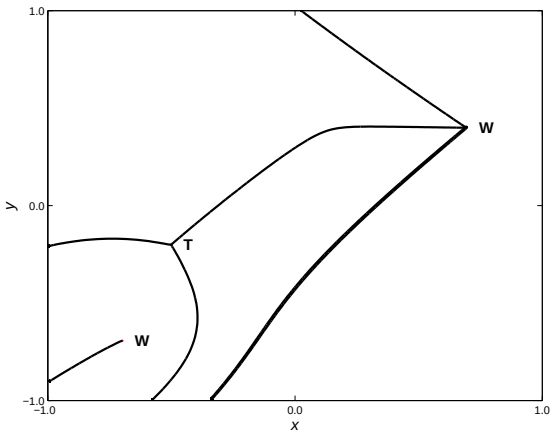

(a) Degenerate points are only classified as the wedge and trisector ('T') types.

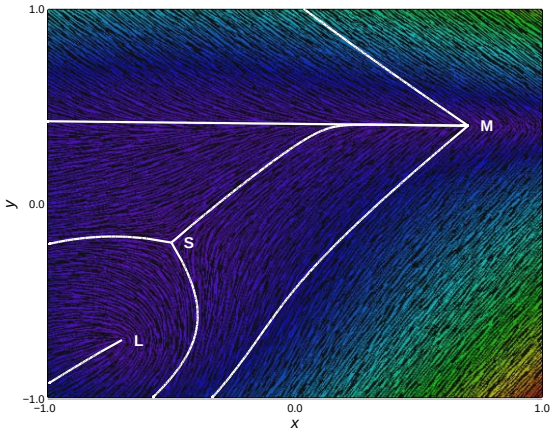

(b) Degenerate points detected by the new algorithm, at $(0.7,0.4)$ there is a monstar type degenerate point.

Figure 7: *Test data set designed from eq. (21)*

5. Conclusions and future works

By extracting the topological structure of the tensor field in the plane, it can greatly reduce the complexity of data to be

visualized and provide a global visualization of the whole field. Furthermore, it can be combined with the icon based method (textures) to enhance the visualization. However, it is important to extract the accurate topological structure, otherwise it will be very misleading.

In this work, we applied theory from the analysis of binary differential equations to address the classification issue of the degenerate point in the existing visualization techniques. In the construction of the topological structure of tensor field, the degenerate point should be classified into three different types: star, monstar and lemon. Lemon is topologically different from monstar. To classify them correctly, a new visualization algorithm is proposed and validated by a synthetic tensor data in this paper.

Last but not the least, in many real cases the tensor fields under study are not generic but satisfy some constraints, often that they must satisfy some system of partial differential equations. In the original case considered by Darboux [Dar96] of the second fundamental form of a surface that tensor indeed statisfies some differential constraints, but nevertheless all three types of degenerate points are observed. In elasticity two common constraints are encountered. A stress-tensor field σ, in the absence of body forces, is said to be *solenoidal* which means $\partial\sigma_{1i}/\partial x_1 + \partial\sigma_{2i}/\partial x_2 = 0$, $i = 1,2$. A strain-tensor field from a small displacement vector field is given by $\varepsilon_{ij} = \partial u_i/\partial x_j + \partial u_j/\partial x_i, i, j = 1,2$, where u_i denote the components of a displacement vector and x_1, x_2 are the basis in the plane, and is said to be *potential*. A necessary and sufficient condition for a tensor field to be potential is the vanishing of the St Venant's tensor [Sha94] in this case is a second order partial differential operator applied to ε_{ij}. In both these important cases all three types of singularities are found. In the future, we will focus on the application of our algorithm on real tensor data arising in these and other applications.

References

[ALGM73] ANDRONOV A. A., LEONTOVICH E. A., GORDON I. I., MAIER A. G.: *Qualitative theory of second-order dynamic systems*. Israel Program for Scientific Translations; [distributed by Halstead Press, a division of] J. Wiley, New York, 1973.

[BF89] BRUCE J. W., FIDAL D. L.: On binary differential equations and umbilics. In *Proceedings of Royal Society of Edinburgh, 111A* (1989), pp. 147–168.

[BH77] BERRY M. V., HANNAY J. H.: Umbilic points on Gaussian random surfaces. *Journal of Physics Annual*, 10 (1977), 1809–1821.

[Car78] CARATHEODORY C.: *Theory of Functions of a Complex Variable*, second ed., vol. one. Chelsea Publishing Company, 1978.

[Dar96] DARBOUX G.: *Leçons sur la theórie générale des surfaces*, vol. IV. Gauthier-Villars, 1896, p. 455.

[Del94] DELMARCELLE T.: *The visualization of second-order tensor fields*. PhD thesis, Stanford University, 1994.

[DH92] DELMARCELLE T., HESSELINK L.: Visualization of second order tensor fields and matrix data. In *VIS '92: Proceedings of the conference on Visualization '92* (1992), IEEE Computer Society Press, pp. 316–323.

[DH94] DELMARCELLE T., HESSELINK L.: The topology of symmetric, second-order tensor fields. In *VIS '94: Proceedings of the conference on Visualization '94* (1994), IEEE Computer Society Press, pp. 140–147.

[HD72] HARDER R., DESMARAIS R.: Interpolation using surface splines. *Journal of Aircraft 9*, 2 (1972), 189–191.

[HH89] HELMAN J., HESSELINK L.: Representation and display of vector field topology in fluid flow data sets. *Computer 22*, 8 (1989), 27–36.

[HH90] HELMAN J., HESSELINK L.: Surface representations of two and three dimensional fluid flow topology. In *VIS '90: Proceedings of the conference on Visualization '90* (1990), IEEE Computer Society Press, pp. 6–13.

[HH91] HELMAN J., HESSELINK L.: Visualizing vector field topology in fluid flows. *IEEE Computer Graphics & Applications 11*, 3 (1991), 36–46.

[Liu08] LIU J.: *The visualization of second rank tensor fields*. PhD thesis, The University of Manchester, 2008.

[LLH97] LAVIN Y., LEVY Y., HESSELINK L.: Singularities in nonuniform tensor fields. In *VIS '97: Proceedings of the conference on Visualization '97* (1997), IEEE Computer Society Press, pp. 59–66.

[LPTH05] LIU J., PERRIN J., TURNER M., HEWITT W.: Perlin noise and 2D second-order tensor field visualization. In *Theory and Practice of Computer Graphics, Eurographics UK Chapter Proceedings* (2005), Eurographics Association, pp. 113–118.

[Por71] PORTEOUS I. R.: The normal singularities of a submanifold. *Journal of Differential Geometry*, 5 (1971), 543–564.

[Por83] PORTEOUS I. R.: The normal singularities of surfaces in $\mathbb{R}^3$. In *Proceedings of Symposis in Pure Mathematics* (1983), vol. 40, pp. 379–393.

[Por01] PORTEOUS I. R.: *Geometric differentiation for the intelligence of curves and surfaces*, second ed. Cambridge University Press, 2001.

[Sha94] SHARAFUTDINOV V.: *Integral Geometry of Tensor Fields*. VSP, Utrecht, 1994.

[SHK*97] SCHEUERMANN G., HAGEN H., KRGER H., MENZEL M., ROCKWOOD A.: Visualization of higher order singularities in vector fields. In *VIS '97: Proceedings of the conference on Visualization '97* (1997), IEEE Computer Society Press, pp. 67–74.

[SHK98] SCHEUERMANN G., HAGEN H., KRÜGER H.: An interesting class of polynomial vector fields. In *Proceedings of the international conference on Mathematical methods for curves and surfaces* (1998), Lillehammer, Norway, pp. 429–436.

[SKMR98] SCHEUERMANN G., KRUGER H., MENZEL M., ROCKWOOD A.: Visualizing nonlinear vector field topology. *IEEE Transactions on Visualization and Computer Graphics 4*, 2 (APRIL-JUNE 1998), 109–116.

[Yu01] YU Z.: Surface interpolation from irregularly distributed points using surface splines, with fortran program. *Computers and Geosciences 27*, 7 (2001), 877–882.

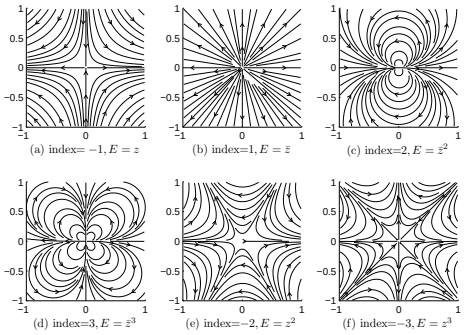

Figure 8: *Examples of vector fields (The notations E, z and $\bar{z}$ will be clarified in the proceeding text.)*

Appendix A: The design of synthetic data

Scheuermann *et al.* [SHK98] proposed a method to construct polynomial vector fields by specifying the critical points and their indices in advance. This method will be used to design the tensor fields on plane as described in section 4. The most important results from the work of Scheuermann *et al.* are now briefly introduced. If $\{\mathbf{e}_1, \mathbf{e}_2\}$ is a basis of $\mathbb{R}^2$, a vector field is defined as:

$$\begin{aligned} &\mathbf{v} : \mathbb{R}^2 \to \mathbb{R}^2 \\ &(x,y) \to \mathbf{v}(x,y) = v_1(x,y)\mathbf{e}_1 + v_2(x,y)\mathbf{e}_2 \end{aligned} \tag{24}$$

Then if $z = x+iy, \bar{z} = x-iy$ are complex numbers in $\mathbb{C}$, then;

$$x = \frac{1}{2}(z+\bar{z}) \tag{25}$$

$$y = \frac{1}{2i}(z-\bar{z}) \tag{26}$$

Thus eq. (24) can be written as:

$$\mathbf{v}(x,y) = v_1\left(\frac{1}{2}(z+\bar{z}), \frac{1}{2i}(z-\bar{z})\right)\mathbf{e}_1 + v_2\left(\frac{1}{2}(z+\bar{z}), \frac{1}{2i}(z-\bar{z})\right)\mathbf{e}_2 \tag{27}$$

and if $\mathbf{e}_1^2 = 1, \mathbf{e}_1\mathbf{e}_2 = i$, $\mathbf{e}_2\mathbf{e}_1 = -i$, then;

$$\begin{aligned} \mathbf{v}(x,y) &= \left[v_1\left(\frac{1}{2}(z+\bar{z}), \frac{1}{2i}(z-\bar{z})\right) - iv_2\left(\frac{1}{2}(z+\bar{z}), \frac{1}{2i}(z-\bar{z})\right)\right]\mathbf{e}_1 \\ &= E(z,\bar{z})\mathbf{e}_1 \end{aligned} \tag{28}$$

where E is a function of z and $\bar{z}$;

$$\begin{aligned} &E : \mathbb{C}^2 \to \mathbb{C} \\ &(z,\bar{z}) \mapsto v_1\left(\frac{1}{2}(z+\bar{z}), \frac{1}{2i}(z-\bar{z})\right) - iv_2\left(\frac{1}{2}(z+\bar{z}), \frac{1}{2i}(z-\bar{z})\right) \end{aligned} \tag{29}$$

Therefore designing a polynomial vector field on $\mathbb{R}^2$ is equivalent to designing a complex-valued function E on $\mathbb{C}^2$, where the critical points of $\mathbf{v}$ are the zeros of $E(z,\bar{z})$. For example, in Figure 8 (a), $E = z$ actually defines a vector field

$$z\mathbf{e}_1 = (x+iy)\mathbf{e}_1 = x\mathbf{e}_1 - y\mathbf{e}_2 = \begin{pmatrix} x \\ -y \end{pmatrix},$$

with a critical point $z = 0$, i.e. $x = y = 0$, which is a saddle with index -1. In comparison, from $E = \bar{z}$, a critical point with index $+1$ can be generated (see Figure 8 (b)). In Figure 8 (c), since $E = \bar{z}^2$, then E has a zero with the multiplicity 2 which defines a vector field shown as dipole $\begin{pmatrix} x^2-y^2 \\ 2xy \end{pmatrix}$ with index $+2$. Scheuermann *et al.* [SKMR98] then introduced the following theorem making it possible to design an analytic vector field with specified positions and topological indices of critical points in $\mathbb{R}^2$.

Theorem A.1 Let $\mathbf{v} : \mathbb{R}^2 \to \mathbb{R}^2$ be an arbitrary polynomial vector field with isolated critical points. Let $E : \mathbb{C}^2 \to \mathbb{C}$ be the polynomial, so that $\mathbf{v}(x,y) = E(z,\bar{z})\mathbf{e}_1$. Let $F_k : \mathbb{C}^2 \to \mathbb{C}, k = 1,\ldots,m$ be the irreducible components of E, so that $E(z,\bar{z}) = \prod_{k=1}^{m} F_k$. Then, the vector fields $\mathbf{w}_k : \mathbb{R}^2 \to \mathbb{R}^2, \mathbf{w}_k(x,y) = F_k(z,\bar{z})\mathbf{e}_1$ have only isolated zeros $z_1,\ldots,z_m$. These are then the zeros of $\mathbf{v}$, and for the Poincaré-Hopf indices we have

$$I_{\mathbf{v}}(z_j) = \sum_{k=1}^{m} I_{\mathbf{w}_k}(z_j) \tag{30}$$

where $I_{\mathbf{v}}(z_j)$ denotes the index of the critical point z_j of the vector field $\mathbf{v}$, and $I_{\mathbf{w}_k}(z_j)$ denotes the index of the critical point z_j of the vector field $\mathbf{w}_k$.

This theorem states two important results. The first is that if a polynomial vector field $\mathbf{v}$ is obtained from a complex-valued function E, the product of the irreducible components F_k, and each F_k further defines a vector field $\mathbf{w}_k$, then each critical point of $\mathbf{w}_k$ will be the critical point of $\mathbf{v}$. The second is that for a critical point at z_j, its index relative to the vector field $\mathbf{v}$ is equal to the sum of indices of z_j relative to each vector field $\mathbf{w}_k$ (see eq. (30)).